Article

The control of acidity in tumor cells: a biophysical model

Nicola Piasentin [§1], Edoardo Milotti[2], and Roberto Chignola[3,*]

[1,2]Department of Physics, University of Trieste, Via Valerio 2, I-34127 Trieste, Italy
[3]Department of Biotechnology, University of Verona, Strada Le Grazie 15 - CV1, I-37134 Verona, Italy
[*]Correspondence: roberto.chignola@univr.it

ABSTRACT Acidosis of the tumor microenvironment leads to cancer invasion, progression and resistance to therapies. We present a biophysical model that describes how tumor cells regulate intracellular and extracellular acidity while they grow in a microenvironment characterized by increasing acidity and hypoxia. The model takes into account the dynamic interplay between glucose and O_2 consumption with lactate and CO_2 production and connects these processes to H^+ and HCO_3^- fluxes inside and outside cells. We have validated the model with independent experimental data and used it to investigate how and to which extent tumor cells can survive in adverse micro-environments characterized by acidity and hypoxia. The simulations show a dominance of the H^+ exchanges in well-oxygenated regions, and of HCO_3^- exchanges in the inner hypoxic regions where tumor cells are known to acquire malignant phenotypes. The model also includes the activity of the enzyme Carbonic Anhydrase 9 (CA9), a known marker of tumor aggressiveness, and the simulations demonstrate that CA9 acts as a nonlinear pH_i equalizer at any O_2 level in cells that grow in acidic extracellular environments.

SIGNIFICANCE The activity of cancer cells in solid tumors affects the surrounding environment in many ways, and an elevated acidity is a common feature of the tumor microenvironment. In this paper we propose a model of intracellular/extracellular acidity that is linked to cellular metabolism and includes all the main molecular players. The model is reliable, robust and validated with experimental data and can be used as an essential building block of more comprehensive *in silico* research on solid tumors.

INTRODUCTION

Acid homeostasis in animal tissues is achieved by active dynamic processes. In physiological conditions, the pH of tissues is maintained between 7.35 and 7.45 in spite of constant metabolic acid production by cells. At the microscopic level, cells must finely regulate their own internal pH to around 7.2 to avoid death (1–3). Cellular acid homeostasis is carried out by active transport of acid/base equivalents across the cell membranes into the extracellular spaces.

Dysregulation of pH is a well-known hallmark of solid tumors (1–3). The tissue of solid tumors is characterized by the presence of an irregular network of blood vessels, causing a spatially heterogeneous delivery of nutrients such as glucose and oxygen to tumor cells (1–4). As the consequence, the inner regions of solid cancers that are distant from blood vessels become hypoxic and acidic. Cancer cells adapt to such adverse environments through a series of molecular changes that involve an increased expression of nutrient and ion transporters and enzymes (reviewed in (1, 3, 5)). For example, hypoxia activates the Hypoxia Inducible Factor-1α (HIF-1α) that up-regulates the transcription of glucose transporters and of enzymes involved in glucose metabolism. Because of hypoxia, glucose is converted mainly to lactic acid through the glycolytic pathway to produce energy under the form of ATP, and the increased production of lactate reduces the pH of the extracellular spaces. A drop in intracellular pH, in turn, increases the activity of lactate and of various ion transporters that collectively contribute to recover intracellular acid homeostasis (1, 3, 5). Hypoxia also causes the increased expression of some membrane-bound enzymes such as Carbonic Anhydrase (CA) that, on the cell surface, catalyzes the hydration of carbon dioxide (CO_2) to protons (H^+) and bicarbonate (HCO_3^-) ions. While the H^+ ions contribute to the acidity of the extracellular milieu, HCO_3^- ions can be transported back into the cells and increase the buffering potential of the intracellular environment (1, 3, 5), further contributing to maintain the intracellular pH at normal values.

It has recently been pointed out (1, 3) that changes in the control of intracellular and extracellular acidity in the tissue of solid tumors are associated with many phenotypic changes of cancer cells with important implications in tumorigenesis, cancer progression, cancer diffusion, escape from immune surveillance and resistance to therapies. For example, microscopic

[§]current address: Department of Chemical and Process Engineering, University of Surrey, GU2 7XH, and Unilever R&D Colworth, Colworth Park, Sharnbook, Bedford MK44 1LQ, UK.

examination of the tumor/normal tissue interface shows that peritumoral acidity drives tumor invasion in the surrounding normal tissue, with the regions of highest tumor invasion corresponding to those of lowest pH. In these regions the environmental pH reaches values that are toxic for normal but not for tumor cells (2).

Biophysical models can help to disentangle the intricate relationships between regulatory biochemical networks and give support to the interpretation of experimental evidence which is rapidly accumulating in this field. In this paper we describe a comprehensive biophysical model of the control of acidity in tumor cells. We study the action of key molecular actors in acid homeostasis of cancer cells, and investigate to which extent hypoxia and environmental acidosis influence their behavior. We focus on the dynamic interplay between lactate, proton, bicarbonate transporters and CA enzyme, and their regulation by oxygen and both extracellular and intracellular pH. The model includes the bicarbonate buffer that acts both in the extracellular and intracellular milieux and it incorporates results from our previous modeling efforts concerning tumor cell metabolism (6–8). In particular, our previous models provide values for the rates of glucose and oxygen uptake, lactate and CO_2 production and lactate/H^+ transport across cell membranes through specific transporters that have already been validated with experimental data. Finally, we fix the model parameters by combining information from a number of experiments carried out with different tumor cell systems.

METHODS

Preliminary considerations and model assumptions

We start from the rather detailed model of tumor cell metabolism and growth that we developed in our previous research (6–8) which successfully reproduces the observed behavior of tumor cells in both liquid (e.g. blood tumors) and solid tumors. In particular, for the current work we have excerpted from that model the part that describes the rates of glucose conversion to lactic acid and oxygen consumption. We remark that the model in (6–8) has been set up with the minimal set of chemical and biochemical pathways that drive the dynamics of metabolism and that are common to most, if not all, tumor cells.

Unlike the metabolic model in (6–8), here we must follow the dynamics of CO_2, HCO_3^- and H^+, both inside and outside a tumor cell. The inputs of the model are the rates of lactate and CO_2 production (fig.1) that depend on how cells take up nutrients, such as glucose, and convert them to ATP through the glycolytic and the oxidative phosphorylation pathways. Lactic acid dissociates immediately to lactate and H^+ ions, and both ions are transported through the cell membrane by means of the bi-directional monocarboxylate transporters MCT (6–8). We remark that this part of the model impacts the rate of change of both intracellular and extracellular pH (from now on pH_i and pH_e, respectively), and oxygen is assumed to diffuse freely through the cell membrane and its consumption rate is used to determine the rate of CO_2 production.

Intracellular H^+ ions are transported outside the cell by means of unidirectional sodium-hydrogen exchangers NHE (1). Different HCO_3^- transporters on the other hand are known to drive the flux of bicarbonate ions through the cell membrane. Some of them import or export HCO_3^- by exchanging Cl^- anions and the transport may depend or not on the presence of Na^+ cations (1). Experimental works, however, have shown that the efficiency of HCO_3^- transport in different cell systems is quite similar, and that the import of HCO_3^- is fundamental in tumor cells where it is dominated by the activity of the Na^+-dependent Cl^-/HCO_3^- exchanger (9, 10). Therefore, we consider the import activity of a generic HCO_3^- transporter ($THCO_3$ in fig.1) which, as a first approximation, assumes the average biochemical characteristics of the Na^+-dependent Cl^-/HCO_3^- exchanger. We finally model the activity of the membrane-bound Carbonic Anhydrase 9 (CA9) enzyme that catalyzes, on the cell surface, the hydration of CO_2. This is an important path since CA9 has been found to be expressed by many solid tumors of different histotypes, and its activity has been correlated to tumor progression and growth (11–13).

We model the kinetics of ion transporters, and of CA9 activity as well, with the Michaelis-Menten/Hill formalism that is described by the following general equation:

$$\frac{d[X]_{C,c}}{dt} = \frac{V_{\max}[X]^h_{C,c}}{K^h_{\mathrm{m}} + [X]^h_{C,c}}$$

where $[X]_{C,c}$ is the molar concentration of a given chemical species inside ($[X]_C$) or outside ($[X]_c$) the cell, V_{max} and K_m are the Michaelis-Menten parameters and h is the Hill exponent ($h > 0$).

We assume that:

- CO_2 can freely diffuse through the cell membrane;
- CO_2 diffusion is driven by the concentration gradient across the membrane and its only important component is the one directed normally with respect to the cell membrane;

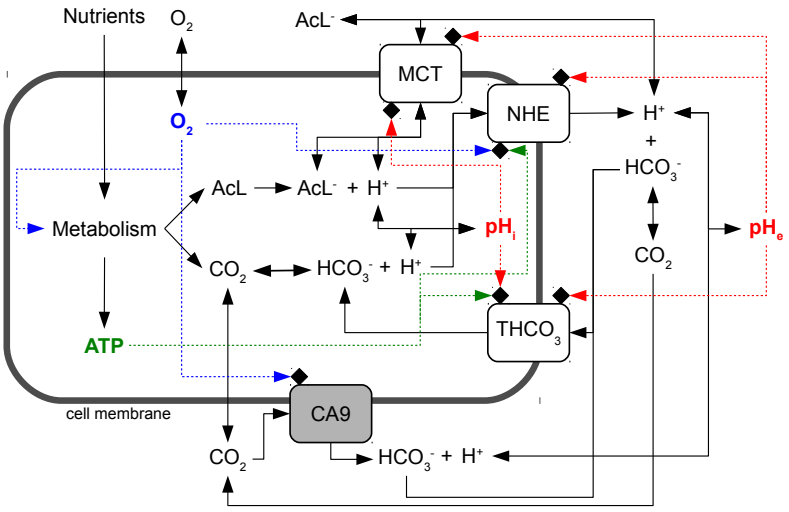

Figure 1: Layout of the model of acidity control in tumor cells. A cell takes up from the environment nutrients and oxygen which are then converted by cell metabolism to lactic acid, CO_2 and ATP. Lactic acid dissociates to lactate and H^+ ions, whereas CO_2 reversibly hydrates to HCO_3^- and H^+. These chemical species diffuse through cell membranes (CO_2) or are actively transported outside and eventually inside the cell by means of specific protein transporters. We consider monocarboxylate (MCT), sodium-hydrogen exchanger (NHE) and generic bicarbonate ($THCO_3$) transporters. We also model the activity of the membrane-bound enzyme Carbonic Anhydrase 9 (CA9). Chemical reactions are indicated by solid lines and the regulatory pathways by dashed lines. Proton concentrations inside and outside the cell are used to compute the intracellular (pH_i) and the extracellular (pH_e) pH. Detailed information on each pathway is given in the main text.

- the diffusion kinetics of charged ions through the cell membrane are much slower than the kinetics of the other processes in which they are involved, and thus the diffusion of charged ions is negligible;
- the mixing of all chemical species in the cell and in the external environment is instantaneous;
- within the short characteristic times of the considered chemical reactions the cell volume is constant.

In this work the variables take the following units for length, mass and time, respectively: μm, pg and s. Molar concentrations (M) have always been converted to mass units by taking into account the volume of the cell (V_C, cell volume is computed by approximating a cell to a sphere of given radius r_C) or of the environment (V_c) and the molecular mass (MW) of chemical species.

Bicarbonate buffer and initial conditions

Central to the whole scheme of reactions shown in fig.1 is the hydration of CO_2. It is well known that at physiologic temperature (i.e. $\sim 37°C$) carbonic acid dissociates very quickly and represents less than 0.5% of the total carbon dioxide and bicarbonate ion (14). Thus, the hydration of CO_2 can be approximated by the following chemical reaction:

$$CO_2 + H_2O \underset{k_1}{\overset{k_2}{\rightleftharpoons}} H^+ + HCO_3^-$$

The values of the two rate constants k_1 and k_2 have been determined in cells under standard culture conditions in two independent experiments with good agreement (11, 15). We take the values in (15): $k_1 \simeq 0.144\ s^{-1}$ and $k_2 \simeq 1.9 \cdot 10^5\ M^{-1}\ s^{-1}$.

We compare model outputs with experimental data obtained with cell cultures *in vitro*, in a standard atmosphere at 37°C and 5% CO_2 at 1 atm pressure. To compute the initial density of CO_2 dissolved in water under these conditions we use Henry's law $c = k(T)P$ where c is the molar concentration of the gas in water, P the pressure and $k(T)$ is a function of temperature

$$k(T) = k^\Theta \exp\left[-\frac{\Delta_{sol}\, k}{R}\left(\frac{1}{T} - \frac{1}{T^\Theta}\right)\right]$$

with $T^{\Theta} = 298.15\,\mathrm{K}$, $k^{\Theta} = 3.3 \cdot 10^{-4}\mathrm{mol\ m^{-3}\ Pa^{-1}}$ and $-\frac{\Delta_{\mathrm{sol}}\, k}{R} = 2400\,\mathrm{K}$ (see ref. (16) for further details); we find that the initial density of CO_2 in cell medium under standard culture conditions is:

$$\rho_{CO_2} = 5.39 \cdot 10^{-5}\ \frac{\mathrm{pg}}{\mu\mathrm{m}^3}$$

Finally, given the CO_2 concentration we find the density of HCO_3^- ions from the Henderson-Hasselbach equation:

$$\mathrm{pH} = \mathrm{pKa} + \log_{10}\left(\frac{[HCO_3^-]}{[CO_2]}\right)$$

where $\mathrm{pKa} = -\log_{10}(k_1/k_2) \simeq 6.12$.

Where not otherwise specified, we fixed the standard intracellular and extracellular pH at 7.4, which determines the initial value of the molar concentration of H^+ ions inside and outside the cells.

CO_2 diffusion through the cell membrane

Given the assumptions above, the component of CO_2 normal to the cell membrane is described by the Fick's first law:

$$J_{1\to 2} = -P_{\mathrm{M},CO_2} \cdot (C_2 - C_1)$$

where $J_{1\to 2}$ is the flux from 1 to 2 in units of concentration over time and surface area S_C, P_{M,CO_2} is the permeability of the carbon dioxide and C_i is the concentration of CO_2 in the i-th volume. Since we model cells grown in an incubator at constant CO_2 pressure, the CO_2 concentration can reach values far from equilibrium only inside cells because of the oxygen consumption by cell metabolism and of the equivalent CO_2 production. This means that in the present model there is only a net outward flux of carbon dioxide from cells to the environment. Thus, the net flux of CO_2 due to diffusion is:

$$\left.\frac{dm_{CO_2,\mathrm{C}}}{dt}\right|_{\mathrm{diff}} = -J_{1\to 2} \cdot \mathrm{MW}_{CO_2} \cdot S_C = P_{\mathrm{M},CO_2}\left(\frac{m_{CO_2,c}}{V_c} - \frac{m_{CO_2,C}}{V_C}\right) S_C \tag{1}$$

MCT transporters

The MCTs are a family of bidirectional H^+ and lactate co-transporters expressed at the cell membrane and their activity has been shown to depend on the pH values on both sides of the cell membrane (see refs. (6–8) and references therein). We model their activity with parameter values extrapolated from experimental observations (6–8) and we use the following equations and parameters to describe the rate of transport of H^+ inside and outside the cell:

$$\begin{aligned} \nu_{\mathrm{MCT}}^{\mathrm{out}\to\mathrm{in}} &= \mathrm{a2c_H} \cdot \frac{\nu_{\mathrm{maxMCT}} \cdot m_{H^+,c}}{V_c K_{\mathrm{mMCT}} + m_{H^+,c}} \\ \nu_{\mathrm{MCT}}^{\mathrm{in}\to\mathrm{out}} &= \mathrm{c2a_H} \cdot \frac{\nu_{\mathrm{maxMCT}} \cdot m_{H^+,C}}{V_C K_{\mathrm{mMCT}} + m_{H^+,C}} \end{aligned} \tag{2}$$

where $\nu_{\mathrm{maxMCT}} = V_{\mathrm{maxAcL}} \cdot \frac{\mathrm{MW_H}}{\mathrm{MW_{AcL}}} \cdot S_C$, $K_{\mathrm{mMCT}} = K_{\mathrm{mAcL}} \cdot \frac{\mathrm{MW_H}}{\mathrm{MW_{AcL}}}$ and where the ratio of molecular weights is used to rescale the equations from concentrations to masses.

In eqns.2, $\mathrm{a2c_H}$ and $\mathrm{c2a_H}$ depend, respectively, on extracellular and intracellular pH, and phenomenologically describe the dependency of MCT transport activity on acidity (for a complete analysis see (6–8)):

$$\begin{aligned} \mathrm{a2c_H} &= 2 - \tanh(\mathrm{a2c_{H\_slope}} \cdot \mathrm{pH}_c - \mathrm{a2c_{H\_thr}}) \\ \mathrm{c2a_H} &= 2 - \tanh(\mathrm{c2a_{H\_slope}} \cdot \mathrm{pH}_C - \mathrm{c2a_{H\_thr}}) \end{aligned} \tag{3}$$

NHE transporters

Sodium-hydrogen exchangers (NHE) are membrane transport proteins that exploit the influx of Na^+ to export H^+ ions. The sodium concentration gradient is maintained by the ATP-dependent Na^+/K^+ pump (17, 18) so that the activity of NHE indirectly depends on ATP availability. This implies that as long as ATP is available the flux of H^+ due to NHE is essentially unidirectional. It has also been reported that NHE activity is inhibited by hypoxia (10, 17) and that, in the long-term, hypoxia inhibits the expression of NHE proteins. Energy and oxygen tune NHE activity and as in the previous model of tumor cell metabolism and growth (6–8), here we take into account these regulatory circuits by means of the two variables SensATP and $\mathrm{Sens}O_2$ that assume real values in the interval [0, 1].

Experimental observations indicate that NHE activity is described by a Hill equation (9, 19, 20) and hence the unidirectional flux of H^+ from the cell to the environment due to NHE transport is modeled by the equation:

$$\nu_{\mathrm{NHE}}^{\mathrm{in}\to\mathrm{out}} = \mathrm{SensATP}\cdot\mathrm{SensO_2}\cdot\mathrm{fpHe_{NHE}}\cdot\frac{\nu_{\mathrm{maxNHE}}\cdot m_{\mathrm{H^+},C}^{h}}{(V_C\cdot\mathrm{MW_H}\cdot K_{\mathrm{mNHE}})^h + m_{\mathrm{H^+},C}^{h}} \tag{4}$$

where $\nu_{\mathrm{maxNHE}} = \mathrm{V_{maxNHE}}\cdot S_C$ and $\mathrm{fPHe_{NHE}}$ is a phenomenological function that tunes the activity of NHE transport as a function of extracellular pH:

$$\mathrm{fpHe} = \frac{1}{2}\left(1 + \frac{\mathrm{pH_e} - \mathrm{pH_0}}{\lambda + |\mathrm{pH_e} - \mathrm{pH_0}|}\right) \tag{5}$$

Indeed, it has been observed that extracellular acidity enhances H^+ transport through NHE (9, 17, 21). In the Supporting Material we discuss how we fix parameter values and define the function fPHe on the basis of experimental observations.

Transport of bicarbonate ions

As discussed above, we model the activity of a generic bicarbonate ion importer (THCO3). The Na^+-dependent Cl^-/HCO_3^- exchanger appears to dominate HCO_3^- fluxes in tumor cells (9, 10), and therefore we take this transporter as a reference to set the values of parameters and fix general biochemical characteristics. This is an important part of the model, because it has been shown that tumor cells do actively import HCO_3^- ions to buffer their internal pH (9, 10), and that this is a common property of different cancer cells. Experimental studies have demonstrated that HCO_3^- import is regulated by both intracellular and extracellular pH but not by hypoxia and that the transport follows a simple Michaelis-Menten kinetics. In the scientific literature there are no indications, as far as we can tell, that HCO_3^- transport depends on ATP availability. However, just as observed for proton export by NHE transporters, HCO_3^- transport proceeds by parallel fluxes of ions, like Na^+ and Cl^-, along their electrochemical gradients that are actively maintained by cells through energy-consuming paths. Thus, it is likely that even HCO_3^- transport is controlled by ATP availability, albeit indirectly. On the basis of these considerations we model HCO_3^- import as follows:

$$\nu_{\mathrm{THCO3}}^{\mathrm{out}\to\mathrm{in}} = \mathrm{SensATP}\cdot\mathrm{fpHe_{THCO3}}\cdot\mathrm{fpHi_{THCO3}}\cdot\frac{\nu_{\mathrm{maxTHCO3}}\cdot m_{\mathrm{HCO_3^-,c}}}{V_c\cdot\mathrm{MW_{HCO3}}\cdot K_{\mathrm{mHCO3}} + m_{\mathrm{HCO_3^-,c}}} \tag{6}$$

where where $\nu_{\mathrm{maxTHCO3}} = \mathrm{V_{maxTHCO3}}\cdot S_C$ and the two functions $\mathrm{fpHe_{THCO3}}$ and $\mathrm{fpHi_{THCO3}}$ phenomenologically describe how HCO_3^- import is affected by extracellular and intracellular pH, respectively. These functions have been fit to actual experimental data (see the Supporting Material) and are modeled by the following equations:

$$\begin{aligned}\mathrm{fpHi_{THCO3}} &= \frac{1}{2}\{1 + \tanh[\gamma_{\mathrm{THCO3}}\cdot(\mathrm{pHi_{0,THCO3}} - \mathrm{pH_i})]\}\\ \mathrm{fpHe_{THCO3}} &= \frac{1}{2}\{1 + \tanh[\lambda_{\mathrm{THCO3}}\cdot(\mathrm{pH_e} - \mathrm{pHe_{0,THCO3}})]\}\end{aligned} \tag{7}$$

Activity of Carbonic Anhydrase 9

The enzyme CA9 is expressed by cells of many different solid tumors, and in general its expression correlates with cancer aggressiveness and poor therapeutic outcome (11–13). It is a membrane-tethered enzyme and it is mainly found at the external surface of cells where it catalyses the hydration of CO_2 (11–13). Importantly, its expression is regulated by hypoxia and indeed CA9 is a marker of hypoxia (22). Again, experimental observations show that CA9 activity follows a Michaelis-Menten kinetics. Thus:

$$\nu_{\mathrm{CA9}} = \mathrm{h_{CA9}}\cdot\frac{\nu_{\mathrm{maxCA9}}\cdot m_{\mathrm{CO_2,c}}}{V_c\cdot\mathrm{MW_{CO2}}\cdot K_{\mathrm{mCA9}} + m_{\mathrm{CO_2,c}}} \tag{8}$$

where where $\nu_{\mathrm{maxCA9}} = \mathrm{V_{maxCA9}}\cdot S_C$ and $\mathrm{h_{CA9}}$ is a phenomenological functions that describe how hypoxia tunes CA9 expression:

$$\mathrm{h_{CA9}} = 3 + 2\cdot\tanh(-\delta_{\mathrm{CA9}}\cdot\mathrm{SensO2}) \tag{9}$$

This is a function of the fraction of available oxygen which, in our model, is defined by SensO2, and it describes the fold change in CA9 expression as observed in actual experiments (see the Supporting Material).

The full model and its numerical integration

The full model is represented by the following set of differential equations:

$$
\begin{aligned}
\frac{dm_{CO_2,C}}{dt} &= gCO_2 - k_1 \cdot m_{CO_2,C} + k_2 \cdot m_{H^+,C} \cdot m_{HCO_3^-,C} \cdot \frac{10^3 \cdot MW_{CO_2}}{V_C \cdot MW_H \cdot MW_{HCO3}} - J_{C\to c} \cdot S_C \cdot MW_{CO_2} \\
\frac{dm_{H^+,C}}{dt} &= gH^+ + k_1 \cdot m_{CO_2,C} \cdot \frac{MW_H}{MW_{CO_2}} - k_2 \cdot m_{H^+,C} \cdot m_{HCO_3^-,C} \cdot \frac{10^3}{V_C \cdot MW_{HCO3}} - \nu_{MCT}^{in\to out} + \nu_{MCT}^{out\to in} - \nu_{NHE}^{in\to out} \\
\frac{m_{HCO_3^-,C}}{dt} &= k_1 \cdot m_{CO_2,C} \cdot \frac{MW_{HCO3}}{MW_{CO_2}} - k_2 \cdot m_{H^+,C} \cdot m_{HCO_3^-,C} \cdot \frac{10^3}{V_C \cdot MW_H} + \nu_{THCO3}^{out\to in} \\
\frac{dm_{CO_2,c}}{dt} &= 0 \\
\frac{dm_{H^+,c}}{dt} &= k_1 \cdot m_{CO_2,c} \cdot \frac{MW_H}{MW_{CO_2}} - k_2 \cdot m_{H^+,c} \cdot m_{HCO_3^-,c} \cdot \frac{10^3}{V_c \cdot MW_{HCO3}} + \nu_{MCT}^{in\to out} - \nu_{MCT}^{out\to in} + \nu_{NHE}^{in\to out} + \nu_{CA9} \cdot \frac{MW_H}{MW_{CO_2}} \\
\frac{m_{HCO_3^-,c}}{dt} &= k_1 \cdot m_{CO_2,c} \cdot \frac{MW_{HCO3}}{MW_{CO_2}} - k_2 \cdot m_{H^+,c} \cdot m_{HCO_3^-,c} \cdot \frac{10^3}{V_c \cdot MW_H} - \nu_{THCO3}^{out\to in} + \nu_{CA9} \cdot \frac{MW_{HCO3}}{MW_{CO_2}}
\end{aligned}
\tag{10}
$$

where $gH^+ = gAcL \cdot MW_H/MW_{AcL}$ and $gCO_2 = qO_2 \cdot MW_{CO_2}/MW_{O_2}$ are, respectively, the rates of H^+ and CO_2 production that are proportional to the rate of lactate production gAcL and oxygen consumption qO_2 as defined in our previous work (6–8), and all the other rates, and regulatory functions, are given in equations 1–9. The multiplicative factor 10^3 that appears in the right-hand side of equations 10 above comes from the conversion of standard molar concentration units to the units used here where masses are expressed in pg and volumes in μm^3.

The system of differential equations 10 is nonlinear and stiff because it incorporates processes with different kinetics, from the fast kinetics of CO_2 hydration and diffusion to the relatively slow kinetics of ion transport and enzyme activity. The system cannot be solved analytically and appropriate numerical approaches are required. We previously investigated this aspect within the context of complex large-scale biophysical models (23) and found that the implicit Euler method is well-suited for the numerical integration of models of this kind. We solved the discretized system of differential equation 10 using the implicit Euler algorithm followed by the Newton-Raphson method to solve numerically the resulting system of nonlinear equations. The code has been implemented in C++ using the computational framework provided by the GNU Scientific Library (24). We used the standard Newton-Raphson solver *gsl_multiroot_fsolver_dnewton* and the *gsl_multiroot_test_residual* library to test the convergence of the algorithm (threshold $\epsilon < 10^{-6}$) within a maximum number of iterations fixed at $N_{max} = 1000$.

RESULTS

The model defined by the set of differential equations 10 has several parameters. We extensively searched the scientific literature to find their values, and when these values were not directly available they were obtained by fit of specific equations to reported experimental data. Experimental evidence was also used to model regulatory functions given by equations 3, 5, 7 and 9 that tune the activity of transporters and CA9 enzyme as the function of local pH, ATP and/or oxygen availability. The full strategy is detailed in the Supporting Material and all parameter values are listed in Table 1.

Once determined, parameter values were fixed and no further tuned to adapt model outputs to data. This means that the model has no free parameters and is strictly predictive. As explained in the next section, for validation purposes we first used it to predict how the intracellular pH (pH_i) varies when cells are grown into environments with increasing acidity.

Model validation with independent experimental data

Model validation was performed with independent experimental data, i.e. data that were not used to set parameter values. To this end we used the data in the paper by Song et al. (28). In this paper Song et al. investigated the dependence of pH_i on pH_e in SCK cells (human choloangiocarcinoma cell line) in standard *in vitro* cultures. Unfortunately, the radius of SCK cells is not reported nor, to the best of our knowledge, it has been measured previously. This is important because our model equations take into account both cell volume (see eqns.1–10) and the cell surface (see e.g. CO_2 diffusion, eq.1) that are both computed from cell radius under the assumption that cell geometry can be approximated by a sphere.

Figure 2 shows the model prediction for intracellular pH vs. cell size, under standard culture conditions. At equilibrium there is a difference of ≈ 0.1 in pH between small and large cells ($r_C = 5.5$ and 8.0 μm, respectively, i.e. a volume ratio of $\simeq 3$)

Table 1: Values of model parameters

Parameter	Value	Unit	Reference
MW_H	1	g mol^{-1}	–
MW_{CO_2}	44	g mol^{-1}	–
MW_{O_2}	32	g mol^{-1}	–
MW_{HCO_3}	61	g mol^{-1}	–
MW_{AcL} [a]	90.1	g mol^{-1}	–
P_{M,CO_2} [b]	3.2×10^4	μm s^{-1}	(25)
gAcL	3.8×10^{-4}	pg s^{-1}	(6)
qO_2	3.5×10^{-5}	pg s^{-1}	(6)
k_1	0.144	s^{-1}	(15)
k_2	1.9×10^5	M^{-1} s^{-1}	(15)
V_{maxAcL}	9.58×10^{-5}	pg s^{-1} μm^{-2}	(8)
K_{mAcL}	0.405×10^{-3}	pg μm^{-3}	(8)
$a2c_H$_slope	1.5	–	(8)
$a2c_H$_thr	7	–	(8)
$c2a_H$_slope	1.5	–	(8)
$c2a_H$_thr	7	–	(8)
V_{maxNHE}	5.15×10^{-7}	pg s^{-1} μm^{-2}	fit of data in (9)
K_{mNHE}	0.196×10^{-6}	M	fit of data in (9)
h	2.67	–	fit of data in (9)
λ_{NHE}	0.076	–	fit of data in (9)
$pH_{0,NHE}$	7.1	–	fit of data in (9)
$V_{maxTHCO3}$	2.02×10^{-5}	pg s^{-1} μm^{-2}	fit of data in (17)
K_{mTHCO3}	7.38×10^{-3}	M	fit of data in (17)
λ_{THCO3}	1.63	–	fit of data in (9)
$pHe_{0,THCO3}$	6.85	–	fit of data in (9)
γ_{THCO3}	4.2	–	fit of data in (10)
$pHi_{0,THCO3}$	6.90	–	fit of data in (10)
V_{maxCA9}	9.47×10^{-2}	pg s^{-1} μm^{-2}	(26)
K_{mCA9}	7.2×10^{-3}	M	(27)
δ_{CA9}	7.3	–	fit of data in (22)

[a] AcL=lactic acid/lactate.

[b] Parameter values have been determined and fixed as described in the Supporting Material section.

but pH_i levels reach values that have actually been observed in tumor cells (28). With the initial conditions discussed above, the simulations approach equilibrium quite fast and this indicates that the numerical solution of model equations is stable.

The model predictions for pH_i values in SCK cells grown in media with increasing acidity are shown in figure 3. We ran simulations with varying cell radius within a range of values which is reasonable for tumor cells, i.e. between 4.5 and 9 μm (29) and computed pH_i at equilibrium. As shown in figure 2 the numerical solutions approach equilibrium with slower kinetics for increasing cell radii. We chose a conservative criterion to define the equilibrium condition and we halted the simulations when $\Delta pH_i/\Delta t < 10^{-5}$ was reached. In these simulations, the volume of the environment was set to $V_c = 10^{12}\mu m^3 = 1mL$, i.e. large enough to assure nearly constant pH_e values throughout the simulation runs. Figure 3 shows that model predictions are in excellent agreement with the experimental data.

Contribution of NHE and THCO3 transporters to pH_i in normoxic or hypoxic environments

We have used the model to study the biochemical mechanisms that allow tumor cells to survive to adverse environments. We have investigated the role of NHE and THCO3 transporters in the control of intracellular acidity by tumor cells exposed to normoxic or hypoxic environments. We ran several simulations by alternatively switching off the activity of NHE and THCO3 transporters, i.e. by setting the respective ν_{max} parameters to 0. The results are shown in figure 4 where we plot the pH_i values at equilibrium (see the previous section) as the function of environmental pH for cells grown under standard oxygen level or at

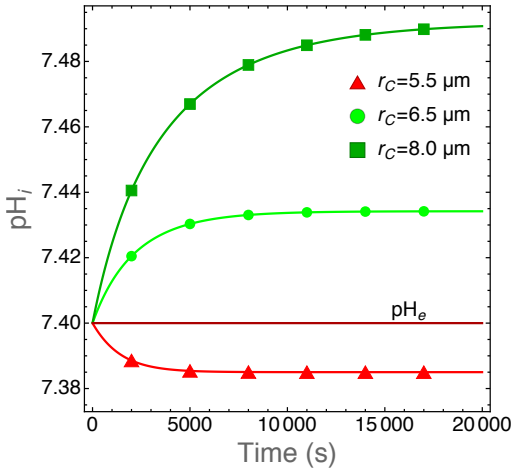

Figure 2: Plot of pH_i as the function of time for cells with the indicated cell radii. We take r_C values that are in the observed range for human tumor cells (29). The model equations have been solved with the parameter values listed in Table 1. After an initial transient, pH_i reach an equilibrium at physiological values and this shows that the model (and its numerical solution) is stable and provides quantitative results in good agreement with actual experimental observations. We also plot pH_e for comparison. The extracellular pH does not vary because these runs were carried out for a limited time span and for cells growing in a large volume (1 mL) filled with fresh medium at physiological pH to mimic standard experimental conditions.

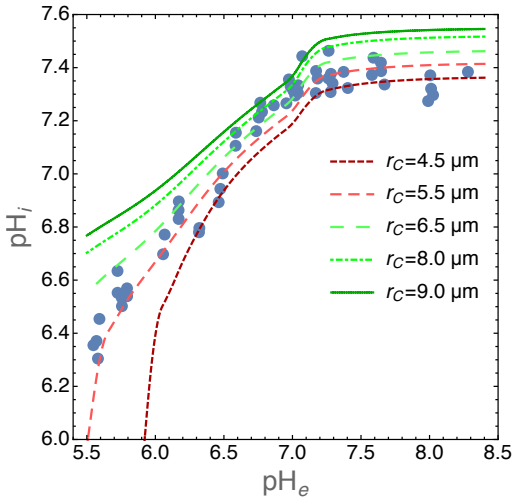

Figure 3: Plot of pH_i for SCK cells grown in media with different pH_e values. Experimental data have been redrawn from figure 2 in (28) (closed circles). The lines show pH_i values at equilibrium as predicted by our model for the indicated cell radii. It is important to note that these are not fits because our model does not have free parameters. Equilibrium was reached at $\Delta pH_i/\Delta t < 10^{-5}$. The volume of the environment was set at $V_c = 10^{12}\mu m^3 = 1mL$.

0.1 fraction thereof.

The simulations clearly show that under normoxic condition the contribution of the THCO3 transporter to pH_i is negligible. Under this condition pH_i is maintained to physiological levels thanks to the activity of NHE transporter that export H^+ ions outside the cells. On the contrary, THCO3 activity dominates in hypoxic environments.

Role of Carbonic Anhydrase 9

As previously noted by Swietach and colleagues (11) pH_i regulation is not affected by CA9 expression in isolated tumor cells, but its role becomes important when cells are grown as three-dimensional aggregates (tumor spheroids). When expressed by

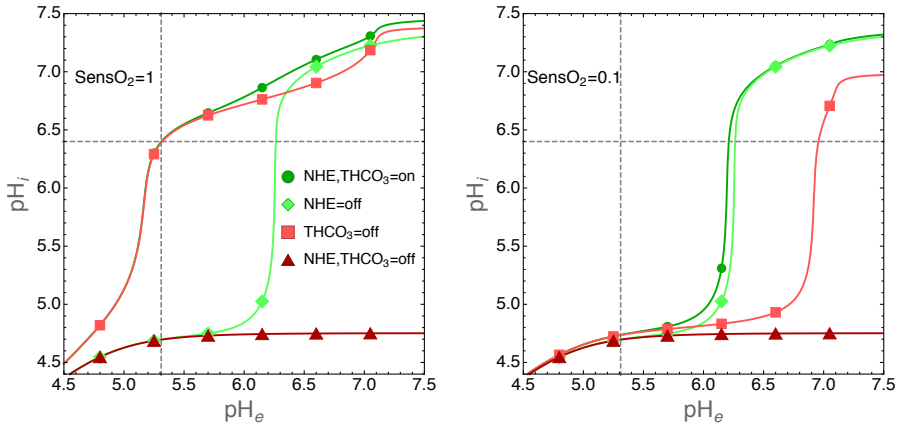

Figure 4: Contribution of NHE and THCO3 transporters to pH_i in normoxic (left panel) or hypoxic (right panel) environments. Simulations were run with the following parameters: cells radius $r_C = 6.5\mu m$ and environmental volume $V_c = 10^{12}\mu m^3$. The intracellular pH was calculated at equilibrium (see also the legend to figure 3) as the function of the indicated pH_e values. The activity of NHE and THCO3 transporters was switched off by setting the respective v_{max} parameters to 0. Environmental oxygen levels were tuned by setting the SensO2 parameter to 1 or to 0.1 (see the Methods section and the Supplementary Material for details). In both panels, dashed lines have been drawn to show the pH_e value at which $pH_i = 6.4$, a value largely compatible with cell life (see also the experimental data in figure 3 for a comparison).

cells grown as tumor spheroids CA9 induces a near uniform intracellular pH throughout the structure (11), an observation that was explained by diffusion-reaction modeling as follows: CA9 coordinates pH_i spatially by facilitating CO_2 diffusion in the unstirred extracellular space of the spheroid (11). This intriguing conclusion, supported by experimental evidence, suggests that CA9 activity becomes important for the control of pH_i by tumor cells at critical sizes of the extracellular volume. We tested this hypothesis with our model, and the results are shown in figure 5.

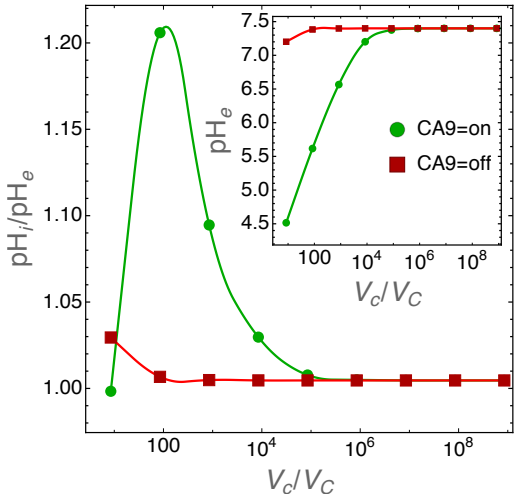

Figure 5: pH_i regulation by CA9 for decreasing size of the extracellular volume. Cell radius was set to the average size of 6.5 μm. The inset shows pH_e values and the main panel pH_i to pH_e ratio for varying V_c/V_C values (i.e. ratio of extracellular to cell volumes) when CA9 activity is turned on or off. In these simulations the extracellular environment is physically closed, i.e. the extracellular volume is unstirred and the diffusion of chemical species toward an "external reservoir" is not allowed.

The role of CA9 in pH_i regulation starts to become important at the extracellular to cell volume ratio $V_c/V_C \approx 10^4$ and reaches a maximum at $V_c/V_C \approx 100$. It is important to note that we simulated cells that grow in a closed environment. This means that at small extracellular volumes the acidity of the environment becomes too high and pH_i runs out of control (see also

figure 4). However, the results in figure 5 show that when $V_c/V_C \approx 100$ and CA9 is active the extracellular pH at equilibrium is around 5.5 and $pH_i \approx 6.6$, well within the physiological range.

Simulations in figure 5 do not take into account the oxygen levels in the tumor environment. As discussed above (see the Methods section) CA9 expression is regulated by hypoxia (22) and thus it is interesting to investigate how pH_i is regulated by cells growing in small environments, i.e. when the CA9 role is not negligible, and when O_2 levels are lower and lower. Figure 6 shows that when $pH_e \geq 5.8$, CA9 acts as a nonlinear pH_i equalizer at any O_2 levels.

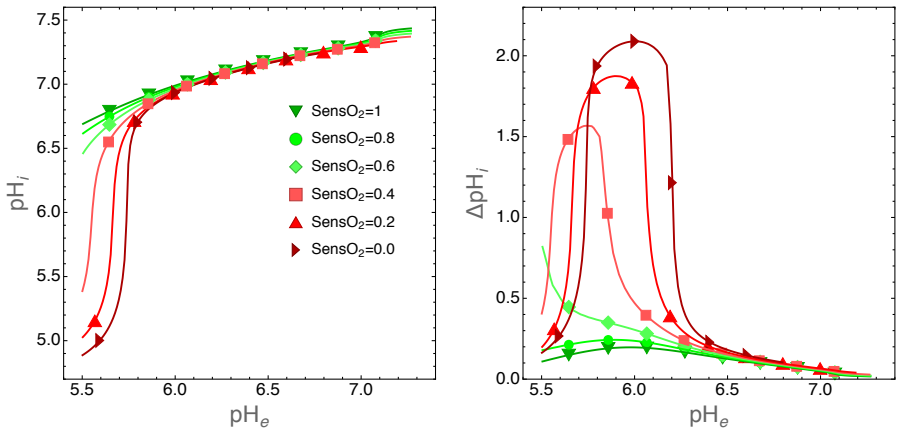

Figure 6: Role of CA9 on pH_i regulation for cells grown in a small environment with decreasing oxygen levels. In these simulations the extracellular volume was set to $V_c = 10^5 \mu m^3$ and cell radius to $r_C = 6.5 \mu m$ so that $V_c/V_C \approx 80$. Left panel: plot of pH_i at equilibrium as the function of pH_e for the indicated fractions of environmental O_2. Right panel: same simulations as those shown in the left panel, but here we plot $\Delta pH_i = pH_{i,CA9=on} - pH_{i,CA9=off}$, i.e. the difference in pH_i when CA9 is turned on or off. This plot clearly shows the nonlinear character of CA9 activity in the regulation of pH_i.

DISCUSSION

We have developed a biophysical model to explore the complex molecular mechanisms that allow tumor cells to regulate both intracellular and extracellular acidity, but we are not alone, other modeling efforts have tried to capture the essential features of the biochemical pathways that lead to acid homeostasis in tumor cells (see e.g. (30–33)). We have taken the remarkable models described in (32) and (33) as our starting point, because of their direct applicability to the analysis of experimental data. The former provides a fully tractable quantitative description of the interplay between H^+ and HCO_3^- transporters with Na^+/K^+-ATPase and Na^+, K^+ and Cl^- ion fluxes, while the latter investigates the interaction of MCT transporters and CA9. We go a few steps further and model the network of important paths that connect together cell metabolism and hypoxia with transport of H^+ and HCO_3^- ions and CA9 activity (see figure 1). The coupling of ion transport mechanisms with metabolism and hypoxia is essential if we want to understand how tumor cells grow and shape their microenvironment, an interplay that is of fundamental importance for the adaptation and evolution of cancer cells within a solid tumor.

We remark that with the model described here we are able to give a quantitative assessment of the importance of specific molecular mechanisms. For instance, simulations show that H^+ efflux from tumor cells dominates the control of intracellular acidity in normoxic environments, whereas HCO_3^- import in hypoxic tumor areas (in our simulation where the fraction of oxygen decrease to 0.1 of standard values). Experiments have shown that in *in vivo* tumor micro-environments oxygen reaches 10% of its normal value at a distance of $\approx 150 \mu m$, i.e. ≈ 10 cell diameters, from blood vessels (34). Thus, within this short distance the control of pH_i is attained by tumor cells through a switch from H^+ export to HCO_3^- import pathways. This observation gives further support to recent work that has shown that inhibition of HCO_3^- fluxes inhibits the growth of experimental tumors by increasing intracellular acidity and cell death (35). When we recall that the hypoxic regions are those where tumor cells show higher resistance to therapies, such as e.g. radiotherapy, then we see that approaches that aim at inhibiting HCO_3^- fluxes would target the very cells that colonize the inner tumor regions and that would otherwise be resistant to therapies, and improve cancer control.

Finally, the model singles out the important role of CA9. The simulations show that CA9 acts as a nonlinear pH_i equalizer at any O_2 level in cells that grow in acidic extracellular environments. This result is in agreement with the experimental observations by Swietach and colleagues (11), collected with tumor spheroids. They observed near-uniform pH_i values

throughout the spheroid structure due to CA9 activity in spheroids grown up to $\approx 500\mu$m diameter. It has long been recognized that tumor spheroids of this size show steep gradients of oxygen with fractions that go as far down as 0 at the center of the spheroid (36). Our simulations show that this is due to the concerted action of CA9 and of hypoxia that up-regulates CA9 expression. These two mechanisms collectively help cells to keep their intracellular pH under control because of increased HCO_3^- production followed by HCO_3^- import through THCO3 transporters.

CONCLUSION

While tumor cell adaptation and survival to extreme microenvironments are key concepts in oncogenesis (1–3), we remark that acid homeostasis is central to cellular adaptation in a much wider context. Active transport of acid/base equivalents across cell membranes into the extracellular spaces may cause transient and rapid changes of microenvironmental and cellular pHs like those observed for other ions involved in cell signalling. Indeed, pH transients have been shown to be important in intra- and inter-cellular communication in the nervous system and are known to affect a number of essential functions, like e.g. neuronal excitability and synaptic transmission (37). This in turn implies that animal cells could sense and adapt to pH changes. The underlying molecular mechanisms are still not well understood, but the role of G-protein coupled receptors in proton sensing is increasingly investigated also in relation to pathological conditions, besides cancer, that result in an increased extracellular acidity, such as infarction and inflammation (38). We conclude that our model can be used as an essential building block of more comprehensive *in silico* research on solid tumors, but it may also help understanding how other cells can sense and dynamically adapt to pH changes.

AUTHOR CONTRIBUTIONS

RC and EM designed the research. RC found parameter values. NP and EM wrote C++ code. NP and RC carried out simulations. RC and EM wrote the article. All authors critically discussed results and revised the article.

REFERENCES

1. Swietach, P., R. D. Vaughan-Jones, A. L. Harris, and A. Hulikova, 2014. The chemistry, physiology and pathology of pH in cancer. *Philosophical Transaction of the Royal Society B* 369:20130099.

2. Estrella, V., T. Chen, M. Lloyd, J. Wojtkowiak, H. H. Cornnell, A. Ibrahim-Hashim, K. Bailey, Y. Balagurunathan, J. M. Rothberg, B. F. Sloane, et al., 2013. Acidity generated by the tumor microenvironment drives local invasion. *Cancer Research* 73:1524–1535.

3. Corbet, C., and O. Feron, 2017. Tumour acidosis: from the passenger to the driver's seat. *Nature Reviews Cancer* 17:577–593.

4. Korenchan, D. E., and R. R. Flavell, 2019. Spatiotemporal pH heterogeneity as a promoter of cancer progression and therapeutic resistance. *Cancers* 11:1026–2069.

5. Fang, J. S., R. D. Gillies, and R. A. Gatenby, 2008. Adaptation to hypoxia and acidosis in carcinogenesis and tumor progression. *Seminars in Cancer Biology* 18:330–337.

6. Chignola, R., and E. Milotti, 2005. A phenomenological approach to the simulation of metabolism and proliferation dynamics of large tumour cell populations. *Physical Biology* 2:8–22.

7. Chignola, R., A. Delfabbro, C. Dalla Pellegrina, and E. Milotti, 2007. *Ab initio* phenomenological simulation of the growth of large tumor cell populations. *Physical Biology* 4:114–133.

8. Milotti, E., and R. Chignola, 2010. Emergent properties of tumor microenvironment in a real-life model of multicell tumor spheroids. *PLoS One* 5:e13942.

9. Hulikova, A., R. D. Vaughan-Jones, and P. Swietach, 2011. Dual role of CO2/HCO3- buffer in the regulation of intracellular pH of three-dimensional tumor growths. *Journal of Biological Chemistry* 286:13815–13826.

10. Hulikova, A., A. L. Harris, R. D. Vaughan-Jones, and P. Swietach, 2013. Regulation of intracellular pH in cancer cell lines under normoxia and hypoxia. *Journal of Cellular Physiology* 228:743–752.

11. Swietach, P., S. Wigfield, P. Cobden, C. T. Supuran, A. L. Harris, and R. D. Vaughan-Jones, 2008. Tumor-associated carbonic anhydrase 9 spatially coordinates intracellular pH in three-dimensional multicellular growths. *Journal of Biological Chemistry* 283:20473–20483.

12. Swietach, P., R. D. Vaughan-Jones, and A. L. Harris, 2007. Regulation of tumor pH and the role of carbonic anhydrase 9. *Cancer and Metastasis Reviews* 26:299–310.

13. Span, P., J. Bussink, P. Manders, L. Beex, and C. Sweep, 2013. Carbonic anhydrase-9 expression levels and prognosis in human breast cancer: association with treatment outcome. *British Journal of Cancer* 89:271–276.

14. Gibbons, B. H., and J. T. Edsall, 1963. Rate of hydration of carbon dioxide and dehydration of carbonic acid at 25. *Journal of Biological Chemistry* 238:3502–3507.

15. Leem, C.-H., and R. D. Vaughan-Jones, 1998. Out-of-equilibrium pH transients in the guinea-pig ventricular myocyte. *The Journal of physiology* 509:471–485.

16. Sander, R., 2015. Compilation of Henry's law constants (version 4.0) for water as solvent. *Atmospheric Chemistry & Physics* 15:4399–4981.

17. Boyer, M. J., and I. F. Tannock, 1992. Regulation of intracellular pH in tumor cell lines: influence of microenvironmental conditions. *Cancer Research* 52:4441–4447.

18. Cassel, D., M. Katz, and M. Rotman, 1986. Depletion of cellular ATP inhibits Na+/H+ antiport in cultured human cells. Modulation of the regulatory effect of intracellular protons on the antiporter activity. *Journal of Biological Chemistry* 261:5460–5466.

19. Jandeleit-Dahm, K., K. M. Hannan, C. A. Farrelly, T. J. Allen, J. R. Rumble, R. E. Gilbert, M. E. Cooper, and P. J. Little, 2000. Diabetes-induced vascular hypertrophy is accompanied by activation of Na+-H+ exchange and prevented by Na+-H+ exchange inhibition. *Circulation Research* 87:1133–1140.

20. Luo, J., D. B. Kintner, G. E. Shull, and D. Sun, 2007. ERK1/2-p90RSK-mediated phosphorylation of Na+/H+ exchanger isoform 1 A role in ischemic neuronal death. *Journal of Biological Chemistry* 282:28274–28284.

21. Alper, S. L., 1991. The band 3-related anion exchanger (AE) gene family. *Annual Review of Physiology* 53:549–564.

22. Wykoff, C. C., N. J. Beasley, P. H. Watson, K. J. Turner, J. Pastorek, A. Sibtain, G. D. Wilson, H. Turley, K. L. Talks, P. H. Maxwell, et al., 2000. Hypoxia-inducible expression of tumor associated carbonic anhydrases. *Cancer Research* 60:7075–7083.

23. Milotti, E., A. Del Fabbro, and R. Chignola, 2009. Numerical integration methods for large-scale biophysical simulations. *Computer Physics Communications* 180:2166–2174.

24. Galassi, M., J. Davies, J. Theiler, B. Gough, G. Jungman, P. Alken, M. Booth, and F. Rossi, 2002. GNU scientific library. *Network Theory Ltd* 3.

25. Missner, A., P. Kügler, S. M. Saparov, K. Sommer, J. C. Matthai, M. L. Zeidel, and P. Pohl, 2008. Carbon dioxide transport through membranes. *Journal of Biological Chemistry* 283:25340–25347.

26. Li, Y., C. Tu, H. Wang, D. N. Silverman, and S. C. Frost, 2011. Catalysis and pH control by membrane-associated carbonic anhydrase IX in MDA-MB-231 breast cancer cells. *Journal of Biological Chemistry* 286:15789–15796.

27. Hilvo, M., L. Baranauskiene, A. M. Salzano, A. Scaloni, D. Matulis, A. Innocenti, A. Scozzafava, S. M. Monti, A. Di Fiore, G. De Simone, et al., 2008. Biochemical characterization of CA IX: one of the most active carbonic anhydrase isozymes. *Journal of Biological Chemistry* 283:27799–27809.

28. Song, C. W., R. Griffin, and H. J. Park, 2006. Influence of tumor pH on therapeutic response. *In* Cancer Drug Resistance, Springer, 21–42.

29. Laget, S., L. Broncy, K. Hormigos, D. M. Dhingra, F. BenMohamed, T. Capiod, M. Osteras, L. Farinelli, S. Jackson, and P. Paterlini-Bréchot, 2017. Technical insights into highly sensitiveIsolation and molecular characterization of fixed and live circulating tumor cells for early detection of tumor invasion. *PloS ONE* 12:e0169427.

30. Webb, S. D., J. A. Sherratt, and R. G. Fish, 1999. Mathematical modelling of tumour acidity: regulation of intracellular pH. *Journal of Theoretical Biology* 196:237–250.

31. Martin, N. K., E. A. Gaffney, R. A. Gatenby, R. J. Gillies, I. F. Robey, and P. K. Maini, 2011. A mathematical model of tumour and blood pHe regulation: the HCO_3^-/CO_2 buffering system. *Mathematical Biosciences* 230:1–11.

32. Bouret, Y., M. Argentina, and L. Counillon, 2014. Capturing intracellular pH dynamics by coupling its molecular mechanisms within a fully tractable mathematical model. *PloS ONE* 9:e85449.

33. Hiremath, S. A., C. Surulescu, S. Jamali, S. Ames, J. W. Deitmer, and H. M. Becker, 2018. Modeling of pH regulation in tumor cells: direct interaction between proton-coupled lactate transporters and cancer -associated carbonic anhydrase. *Mathematical Biosciences and Engineering* 16:320–337.

34. Helmlinger, G., F. Yuan, M. Dellian, and R. K. Jain, 1997. Interstitial pH and pO_2 gradients in solid tumors *invivo*: high-resolution measurements reveal a lack of correlation. *Nature Medicine* 3:177–182.

35. McIntyre, A., A. Hulikova, I. Lefaki, C. Snell, D. Singleton, G. Steers, P. Seden, D. Jones, E. Bridges, S. Wigfield, J.-L. Li, A. Russell, P. Swietach, and A. H. Harris, 2016. Disrupting hypoxia-induced bicarbonate transport acidifies tumor cells and suppresses tumor growth. *Cancer Research* 76:3744–3755.

36. Mueller-Klieser, W., 1984. Method for the determination of oxygen consumption rates and diffusion coefficients in multicellular spheroids. *Biophysical Journal* 46:343–348.

37. Deitmer, J. W., and C. R. Rose, 1996. pH regulation and proton signalling by glial cells. *Progress in Neurobiology* 48:73–103.

38. Zhu, H., X. Cheng, X. Niu, Y. Zhang, J. Guan, X. Liu, S. Tao, Y. Wang, and C. Zhang, 2015. Proton-sensing GPCR-YAP signalling promotes cell proliferation and survival. *International Journal of Biological Sciences* 11:1181–1189.